EE

GSI-94-41
PREPRINT
JULI 1994

FIRST SPATIAL ISOTOPIC SEPARATION OF RELATIVISTIC URANIUM PROJECTILE FRAGMENTS

A. MAGEL et al.

(Submitted to Nucl. Instr. and Meth. in Phys. Res. B)

ellschaft für Schwerionenforschung mbH
ach [illegible] 52 D-64220 Darmstadt Germany

First Spatial Isotopic Separation of Relativistic Uranium Projectile Fragments

A. Magel [b,a,1], H. Geissel [a], B. Voss [c], P. Armbruster [a], T. Aumann [d], M. Bernas [e], B. Blank [f], T. Brohm [c], H.-G. Clerc [c], S. Czajkowski [a], H. Folger [a], A. Grewe [c], E. Hanelt [c], A. Heinz [c], H. Irnich [a], M. de Jong [c], A. Junghans [c], F. Nickel [a], M. Pfützner [g], A. Piechaczek [a], C. Röhl [c], C. Scheidenberger [a], K.-H. Schmidt [a], W. Schwab [a], S. Steinhäuser [c], K. Sümmerer [a], W. Trinder [a], H. Wollnik [b], G. Münzenberg [a]

[a] *Gesellschaft für Schwerionenforschung, D-64291 Darmstadt, Germany*

[b] *II. Physikalisches Institut, Gießen University, D-35392 Gießen, Germany*

[c] *Technische Hochschule Darmstadt, D-64289 Darmstadt, Germany*

[d] *Institut für Kernchemie, Mainz University, D-55099 Mainz, Germany*

[e] *Institut de Physique Nucléaire, Orsay, IN2P3, France*

[f] *CENBG, 33175 Gradignan CEDEX, France*

[g] *Institute of Experimental Physics, Warsaw University, Warsaw, Poland*

Abstract

Spatial isotopic separation of relativistic uranium projectile fragments has been achieved for the first time. The fragments were produced in peripheral nuclear collisions and spatially separated in-flight with the fragment separator FRS at GSI. A two-fold magnetic-rigidity analysis was applied exploiting the atomic energy loss in specially shaped matter placed in the dispersive central focal plane. Systematic investigations with relativistic projectiles ranging from oxygen up to uranium demonstrate that the FRS is a universal and powerful facility for the production and in-flight separation of monoisotopic, exotic secondary beams of all elements up to Z = 92. This achievement has opened a new area in heavy-ion research and applications.

[1] Work done in partial fulfillment of the requirements for the doctoral degree, University of Gießen

submitted to NIM B

1 Introduction

In first experiments with relativistic beams of light projectiles up to calcium at the BEVALAC in Berkeley [1,2] it was demonstrated that projectile fragmentation is a powerful mechanism to produce new exotic nuclei. Intermediate-energy light secondary beams became an important tool in nuclear-structure research and are meanwhile used in several laboratories, like GANIL, MSU, and RIKEN which have devoted a major part of their experimental program to this field. In order to study and to use a projectile-fragment beam it must be purified by a suitable separation technique. The separation methods developed at the BEVALAC have been refined and applied in the other laboratories mainly for beams up to medium masses [3]. Recently, new possibilities have opened up at GSI for secondary-beam experiments at high energies; the separation of monoisotopic exotic beams up to gold has been achieved by the projectile fragment separator FRS [4,5]. The spatial in-flight separation is a prerequisite to effectively combine a secondary beam facility with other ion-optical devices, e.g. with a storage-cooler ring [6].

The FRS [4] was designed to provide isotopically pure secondary beams of all elements up to Z = 92 in the energy range of 100-2000 A·MeV. The device is fully integrated in the high-energy facilities at GSI, see fig. 1. The projectiles are accelerated by the heavy-ion synchrotron SIS [7] and produce the exotic nuclei of interest in the production target placed at the entrance of the FRS.

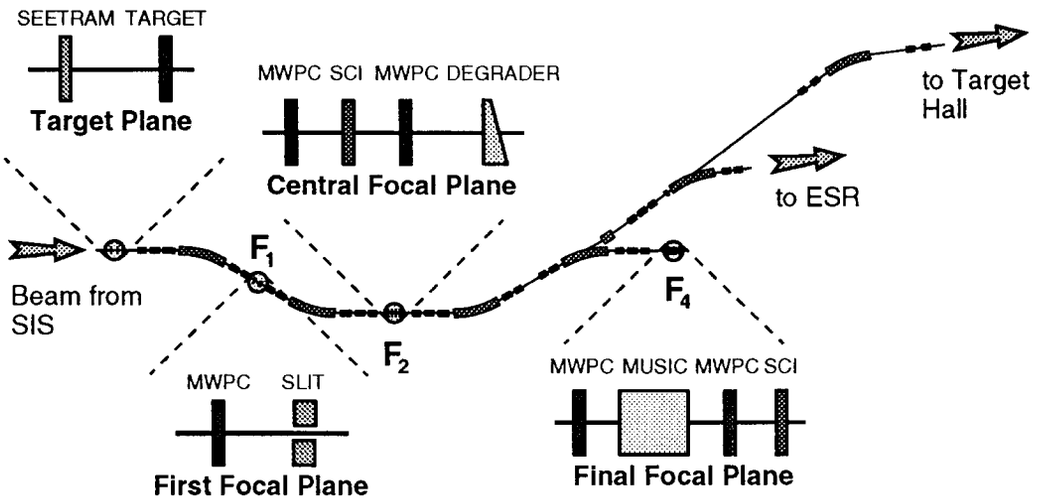

Fig. 1. Layout of the projectile fragment separator FRS [4] at GSI. The secondary beams produced in the target can be investigated at the central and final focal planes, F_2 and F_4, respectively. They can be also injected into the storage-cooler ring ESR or directly transported to the target-hall facilities. The figure also shows the standard detector setup for particle identification used at the target and at the F_1, F_2, and F_4 areas. The abbreviations used to denote the different detectors are explained in section 3 of this article.

The fragments are separated in-flight to be investigated directly in the FRS, in the storage-cooler ring ESR [8], or in any of the detector facilities in the target hall.

In this paper we present results demonstrating the performance of the FRS for the most difficult case, the separation of uranium fragments, which successfully terminates a first series of secondary-beam experiments with projectiles from oxygen up to uranium.

2 Isotopic separation of relativistic projectile fragments

Electromagnetic dissociation (EMD) and fragmentation of heavy ions are the dominant nuclear reactions at relativistic energies for the efficient production of secondary nuclear beams.

EMD occurs at impact parameters larger than the sum of the radii of the two colliding nuclei. High-lying collective modes (the giant resonances), can be excited with very large cross sections. The excited projectile nuclei decay via photon or nucleon emission, or, as in the case of uranium beams, also by fission. EMD is a cold reaction process which produces fragments close to the mass of the projectile, or fission fragments for the heaviest elements.

Fragmentation occurs at impact parameters for which the radii of the interacting nuclei overlap. During the short nuclear encounter between projectile and target several nucleons can be abraded leading to a highly-excited prefragment. In the slower deexcitation step it decays mainly via evaporation of nucleons. The fragmentation process can provide nuclei far off stability.

Projectile fragments at relativistic energies are characterized by favorable kinematics for in-flight separation: The fragment velocity is close to that of the projectile, and the parallel and longitudinal momentum distributions are narrow, i.e. the fragments are emitted in a narrow angular cone (< 1 degree), thus the emittance of the fragment beam is small. Due to these properties, forward spectrometers are well suited to collect and to separate these reaction products and inject them into other ion-optical devices [9].

The FRS [4] is an achromatic forward spectrometer that consists of four identical sections each equipped with a 30 degree dipole magnet, a magnetic quadrupole triplet, and a doublet. Magnetic hexapoles placed directly in front of and behind each dipole are used to correct second-order image aberrations. The ion-optical system can be operated in the range of magnetic rigidities between 5 and 18 Tm. In the standard achromatic mode of the FRS the target is 2.28 m in front of the first quadrupole triplet resulting in an acceptance

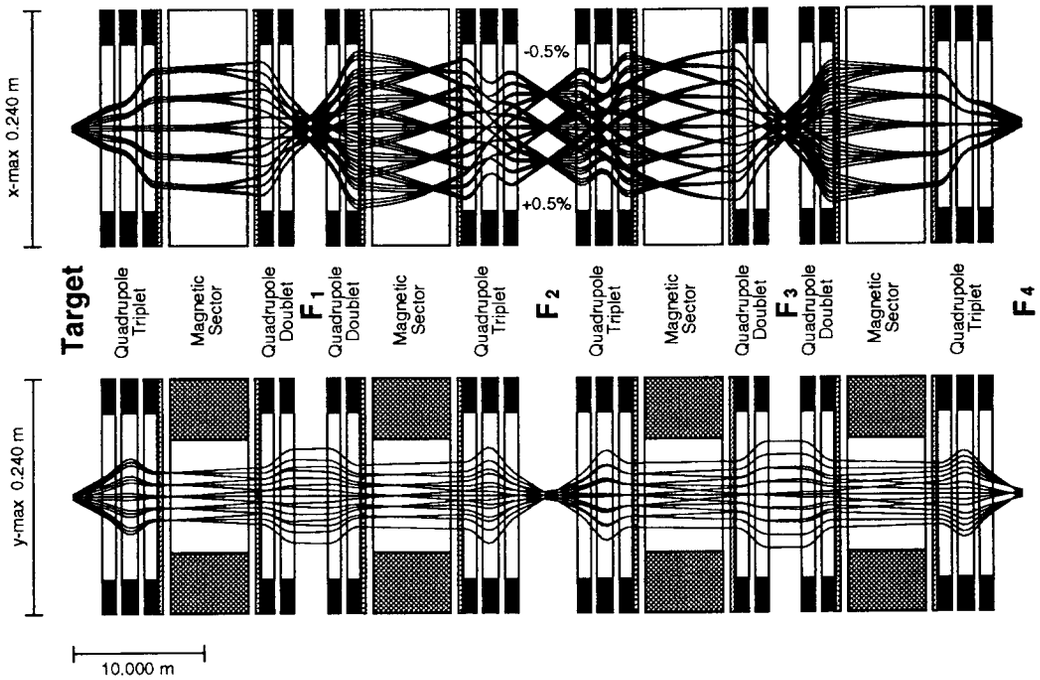

Fig. 2. Ion-optical layout of FRS in the achromatic standard mode [4] calculated in third order with the program GICO [10]. The upper figure shows the trajectories of ions in the dispersive direction (x) starting at the entrance with three different positions, five different angles, and three different momenta ($\frac{\Delta p}{p} = -0.5\%, 0\%, +0.5\%$). The lower part shows the corresponding trajectories in the perpendicular direction (y).

of $20\,\pi$ mm mrad in horizontal (x) and $40\,\pi$ mm mrad in vertical (y) direction together with an acceptance in momentum of $\Delta p/p = 2\%$. Since the typical beam spot at the target is 2-3 mm wide, the dispersion of 6.8 cm/% in the central focal plane allows a Bρ-resolving power of 1600.

Figure 2 illustrates the ion-optical layout of the system. In this third-order calculation with the program GICO [10] the field strengths of the hexapoles are tuned to minimize the second order image aberrations and to orient the focal planes at F_2 and F_4 perpendicular to the optical axis.

The pure magnetic-rigidity analysis selects all projectile fragments that have a similar mass-to-charge ratio, since these reaction products have approximately the same velocity. For fully-ionized fragments this separation corresponds to an A/Z selection. To achieve a spatial isotopic separation, a second independent selection criterion is necessary. This is done by using in addition the atomic slowing-down within a thick layer of matter. An energy degrader is placed in the dispersive plane F_2. The following two dipole stages analyze the atomic energy loss (ΔE). This combined Bρ-ΔE-Bρ analysis allows a spatial separation according to nuclear mass and charge [4,11,12]. The best separation can be achieved if the energy degrader is shaped such that the achromatism

of the ion-optical system is preserved. The selected thickness of the degrader is usually about half of the range of the fragment. The degrader can also be shaped to allow an optimum energy bunching. This is needed if the fragments are to be studied after implantation in thin detectors or for applications of radioactive tracer beams [12,13].

Using this separation method requires a precise knowledge of the atomic interactions of heavy ions in matter. The Bρ-ΔE-Bρ method is most effective if the energy of the fragments is high enough to ensure that the ions emerging from the production target or from the thick energy degrader are completely ionized. Fragments in several charge states cause ambiguities in the Bρ analysis. Due to the high resolving power of the FRS the system is very sensitive to a precise prediction of the energy loss of the heavy ions in the different layers of matter. Uncertainties of the order of 10^{-2} are not tolerable for the magnetic field setting after the thick degrader since the dispersion of the second half of the FRS of 8.62 cm/% would lead to a misalignment of the secondary beam at the final focal plane of the spectrometer. Careful calibration of the thicknesses of all materials are performed by energy-loss measurements with the primary beam before the magnetic field strengths are scaled to the predicted rigidity for the desired fragments. We have performed experiments with the FRS to study the atomic charge-exchange and energy-loss processes to predict and optimize the separation [14,15].

Our results from the atomic-collision studies are implemented in the ion-optical program MOCADI [16] which is used to calculate the magnetic field strengths and the degrader properties for a selected fragment beam. MOCADI simulates the transport of relativistic heavy ions through matter and ion-optical systems. The ion-optical description is based on third-order transfer matrices calculated by the program GICO. Detectors, targets, apertures and other mechanical dimensions (chambers, vacuum tubes etc.) can be taken into account in the ray-tracing calculation to predict a realistic ion-optical transmission for exotic beams through the FRS.

The separation efficiency calculated with MOCADI includes the ion optical transmission of the separator and losses due to nuclear reactions of the secondary beam passing matter. The nuclear absorption in the production target, degrader, detectors, vacuum windows etc. are implemented by using the Kox formula [17] for the total reaction cross section, the EPAX prediction [18] for the production cross section of the specific fragment, and the electromagnetic dissociation according to Bertulani and Baur [19]. The kinematics of projectile fragmentation is included by the systematics of Morrissey [20]. MOCADI allows to simulate most experimental conditions and to compare measured spectra such as position distributions, time-of-flight and energy-loss spectra with the calculated ones. Besides preparing and guiding a secondary-beam experiment, the calculated spectra can be used to deconvolute the different

contributions of the measured spectra, e.g. to disentangle the atomic and nuclear interactions in the measured momentum distributions.

The isotopic resolving power of the fragment separator has been successfully verified in several experiments with primary beams ranging from oxygen to gold at energies between 300 and 1000 A·MeV [4]. The level of difficulty increased with increasing Z of the projectile due to the fact that with smaller relative mass differences between neighboring isotopes the separation becomes more sensitive to aberrations of the ion-optical system as well as to the imaging and separation properties of the degrader system. Thickness inhomogeneities of the target, degrader and detectors and the resulting straggling as well as incomplete electron stripping are further complications for the heavier projectile fragments. A uranium beam is the crucial test case for the isotopic separation of the heaviest possible projectile fragments.

3 Spatial separation of uranium projectile fragments

The goal of the present experiment was to produce and to separate uranium fragments at the highest energy available from SIS. The projectiles were extracted in the charge state 73^+ at an energy of 950 A·MeV which is close to the maximum magnetic rigidity of the synchrotron. The charge state accelerated is determined by the ionic charge-state distribution behind the stripper foil in the transfer beamline between the linear accelerator UNILAC and SIS at an injection energy of 11.4 A·MeV. Already from the first experiments on charge exchange processes of the heaviest ions at the BEVALAC [21] it could be deduced that even at 1 A·GeV hydrogen-like and helium-like ionic states contribute significantly to the equilibrium charge state distribution of uranium ions. As outlined in the previous section, the requirement for an unambiguous isotopic separation using the Bρ-ΔE-Bρ identification alone is therefore not fulfilled for the present experiment. In the first part of the experiment we have therefore investigated the equilibrium charge state distribution of uranium projectiles at different energies penetrating different target materials.

3.1 Charge-state distributions of uranium ions

Several targets between beryllium and lead were mounted in the target station at the entrance of the FRS. Their thicknesses (several hundred mg/cm^2) were selected such that the emerging charge-state distribution is independent of the incident charge state, i.e. the equilibrium charge-state distribution is obtained. Behind the target the uranium projectiles were separated according to their charge state by the first dipole magnet and recorded event-by-event using the

multiwire proportional counter (MWPC) installed at the first focal plane F_1 which is part of the standard diagnostics of the FRS. The results for uranium projectiles at 950 A·MeV are presented in fig. 3. This figure shows the measured charge-state fractions after penetrating different target materials. The lines in this plot represent a theoretical prediction based on high-energy approximations [23,22].

The experimental results demonstrate that the highest abundance of fully stripped uranium ions is obtained by penetrating medium to high Z target materials. This behavior is determined by the different energy- and Z-dependences of the two different electron capture processes, the radiative electron capture and the kinematical electron capture. The radiative electron capture is dominant for light targets. It is striking how reliably the theory can reproduce the data at a fixed velocity in the different target materials.

The criteria for selecting an efficient fragmentation target are: 1. High density of target atoms, 2. small energy and angular straggling, and 3. high electron stripping efficiency. The conditions 1 and 2 require low-Z targets like beryllium whereas the last condition, which is very important for the heaviest projectile beams, requires a heavy material. We have chosen a copper target as a suitable

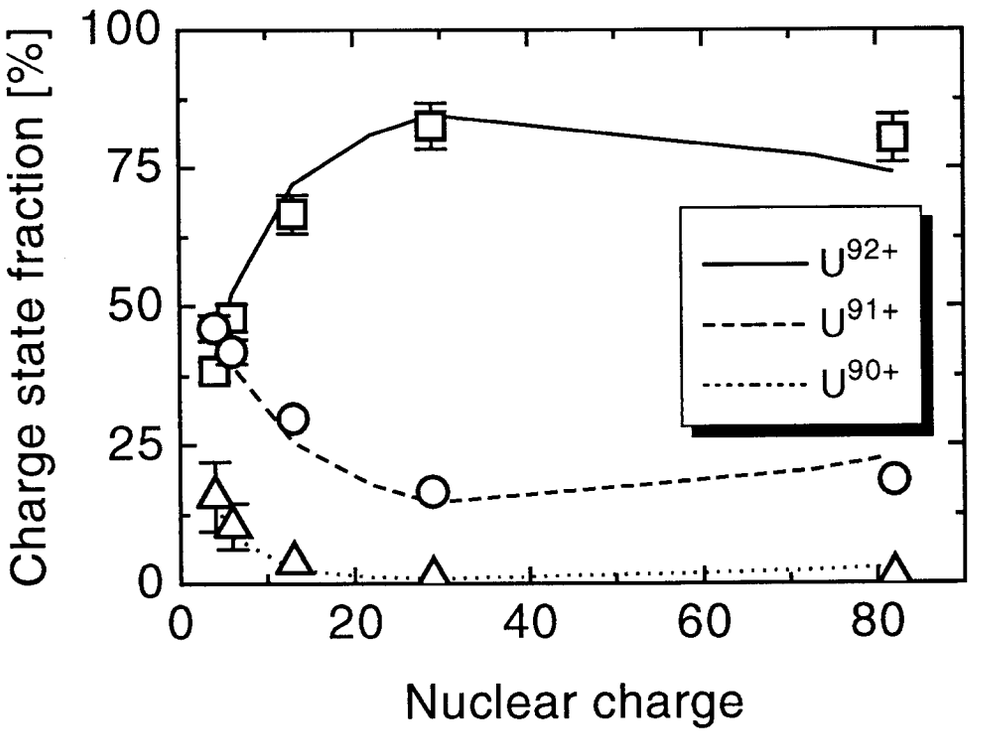

Fig. 3. Measured equilibrium charge-state distributions (symbols) of a 950 A·MeV uranium beam as a function of the nuclear charge of the target. The data are compared to theoretical predictions (lines) [22].

compromise, since its stripping efficiency is only slightly below that of lead, see fig. 3, but its atomic straggling effects are much smaller.

In fig. 4 we show the measured equilibrium charge-state distribution for uranium ions emerging from copper targets over a wide energy range, again compared to theoretical predictions. The experimental results agree quite well with theory. Furthermore, it can be seen that only about 80% of 950 A·MeV uranium ions are fully ionized which means that hydrogen-like and helium-like charge states of U projectile fragments will inevitably be superimposed in the Bρ-ΔE-Bρ separation.

In future experiments the contaminants due to incomplete electron stripping can be further reduced by increasing the energy of the initial beam, see fig. 4. In principle this is possible by accelerating the projectiles in higher charge states. This can be reached by stripping the extracted SIS beam to 92^+ and reinjecting the uranium beam via the ESR into the synchrotron. At the time of our experiment this option was not available. Future post-acceleration in SIS will then provide fully ionized uranium at a maximum energy of 1350 A·MeV, this would reduce the intensities in the hydrogen- and helium-like charge states below 8% [22].

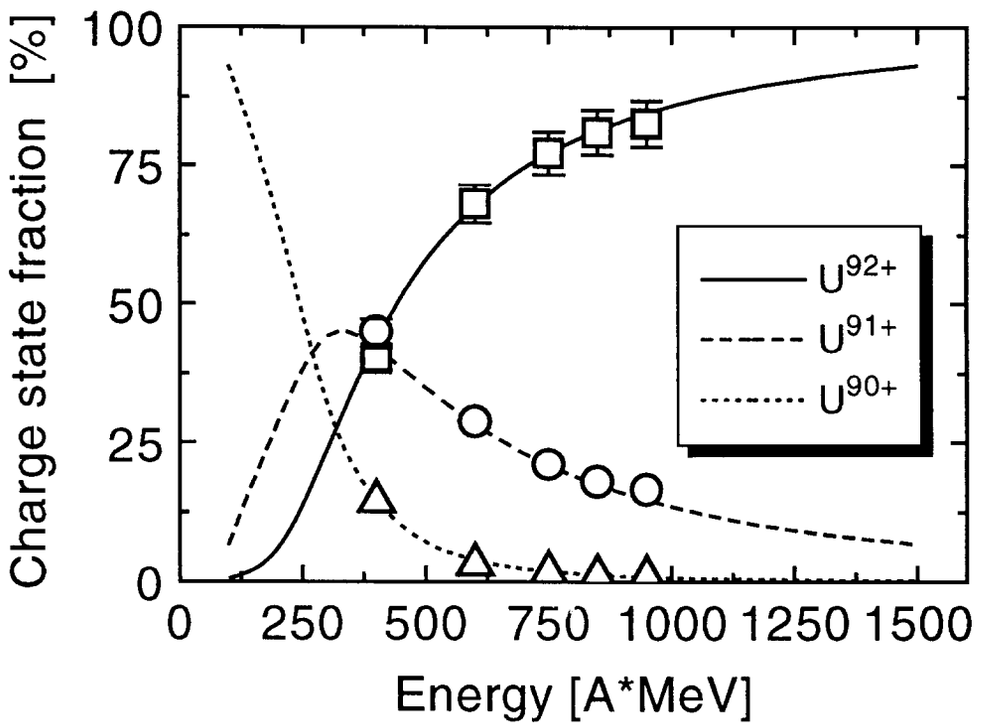

Fig. 4. Measured equilibrium charge-state distributions (symbols) of a ^{238}U beam after penetrating a copper target as a function of the incident energy [14]. The data are compared to theoretical predictions (lines) [22].

3.2 Experimental procedure for the spatial isotopic separation

A main aim of the experiment was to demonstrate the isotopic separation power of the FRS for the heaviest fragments at relativistic energies. As an example we selected the isotope ^{236}U produced in peripheral collisions of 950 A·MeV ^{238}U projectiles in a 205 mg/cm^2 copper target. The beam was slowly extracted from SIS with a pulse length of 2 s and an intensity of 10^6 ions/spill which was measured by a secondary-electron transmission monitor (SEETRAM) [24,25]. The diameter of the beam spot at the target was about 2.5 mm (FWHM) both in horizontal and in vertical direction.

The first two dipole stages of the FRS were tuned to a magnetic rigidity of 13.851 Tm to center the isotope ^{236}U on the optical axis of the spectrometer, this setting corresponds to an A/Z ratio of 2.566. The magnetic field strengths of the bending magnets were measured with an accuracy of 10^{-4} using calibrated Hall probes. The magnetic rigidity of ^{238}U behind the production target differed by 0.8% from that of ^{236}U. Therefore, we used the horizontal slits at the first focus F_1 to stop the primary beam. To obtain spatial isotopic separation a degrader was mounted at the central focal plane F_2 [26]. The effective thickness of the matter in the F_2 section was 5300 mg/cm^2 of aluminum comprising the degrader itself as well as the corresponding thicknesses of the scintillation detector in air and the vacuum windows. The position-sensitive scintillator [27] served as a start detector for time-of-flight (TOF) measurements and for the determination of the Bρ of each fragment to extract the A/Z ratio. The selected fragment ^{236}U was slowed down in the degrader to an energy of 542 A·MeV, and therefore the third and the fourth dipole stage of the FRS were tuned to a Bρ value of 9.773 Tm. The achromatism of the FRS was conserved by adjusting the slope of the degrader to -5.31 mrad in the dispersive direction. Behind the degrader only about 47% of the uranium fragments are fully ionized. The H- and He-like charge states are populated to about 42% and 11%, respectively, see fig. 4.

We have measured the position spectra of the fragments at the central focal plane F_2 and the final focal plane F_4 event-by-event. The position information was obtained by measuring the time difference between the two light signals on both sides of the scintillator. The resolution obtained was about 50 ps (FWHM) which corresponds to a spatial resolution of 4 mm (FWHM). The position calibration was achieved by using MWPC detectors that are part of the standard beam diagnostics of the FRS [28]. During the experiment the MWPC were removed because their thickness inhomogeneities resulting from the 50 μm wire planes would deteriorate the resolution of the spectrometer.

To verify the expected isotope distribution the fragments had to be identified with respect to A and Z. The magnetic rigidity of the particles in the second

half of the FRS was determined by the magnetic field strengths of the corresponding bending magnets and by the horizontal position of the ions at F_2 and F_4. The mass-to-charge ratio was determined by measuring the time-of-flight for the path length of about 34 m. The time resolution achieved was better than 90 ps (FWHM). Finally, the nuclear charge of the ions was determined by their energy-deposition in a MUltiple-Sampling Ionization Chamber (MUSIC) [29] mounted at the exit of the separator, see fig. 1.

3.3 Results for the separation of ^{236}U

Figure 5 shows the measured position of the fragments at the central focal plane plotted versus the corresponding position at the final focal plane. The desired nuclide ^{236}U is centered in both planes, and the islands visible along a diagonal above and below represent other fully-ionized uranium isotopes. A small portion of the primary beam that was not completely removed by the slits at F_1 is still visible. At the left-hand side of the figure one can see a shifted image of this isotope distribution. It consists of uranium fragments that left the production target fully ionized, but left the degrader in the hydrogen-like charge state. Due to the dispersion of the second half of the FRS of 8.62 m they are shifted by 95 mm relatively to the uranium nuclides which were fully ionized. The weak islands in between these two dominating chains are mainly bare protactinium isotopes. The ions to the right side of U^{92+} represent uranium isotopes which left the production target in a hydrogen-like charge state and kept one electron behind the degrader.

By using the time-of-flight (TOF) and the energy-deposition in the MUSIC chamber it is possible to remove the contaminants due to incomplete stripping of the ions in the offline analysis. In figure 6a the contaminants due to different ionic charge states are removed, and the fragments are spatially well separated. The mass resolution of the FRS deduced from this spectrum corresponds to $A/\Delta A \approx 240$. On the left hand side of the spectrum the row of the thorium isotopes is now visible. In figure 5 it was completely covered by uranium fragments in the H-like ionic charge state. This shows that by using both the time-of-flight and the energy-deposition information it is possible to suppress the background due to incomplete stripping by several orders of magnitude.

The velocity spread of the fragments determines the efficiency and the resolution of the pure spatial separation. The spread is caused by nuclear reactions and by the atomic energy-loss straggling. In addition, one must take into account the energy spread caused by the stopping-power difference of the projectiles and the fragments due to the depth of the nuclear reaction within the thick production target. The energy straggling induced by the degrader is a main contribution to the width of the position distributions at F_4. The

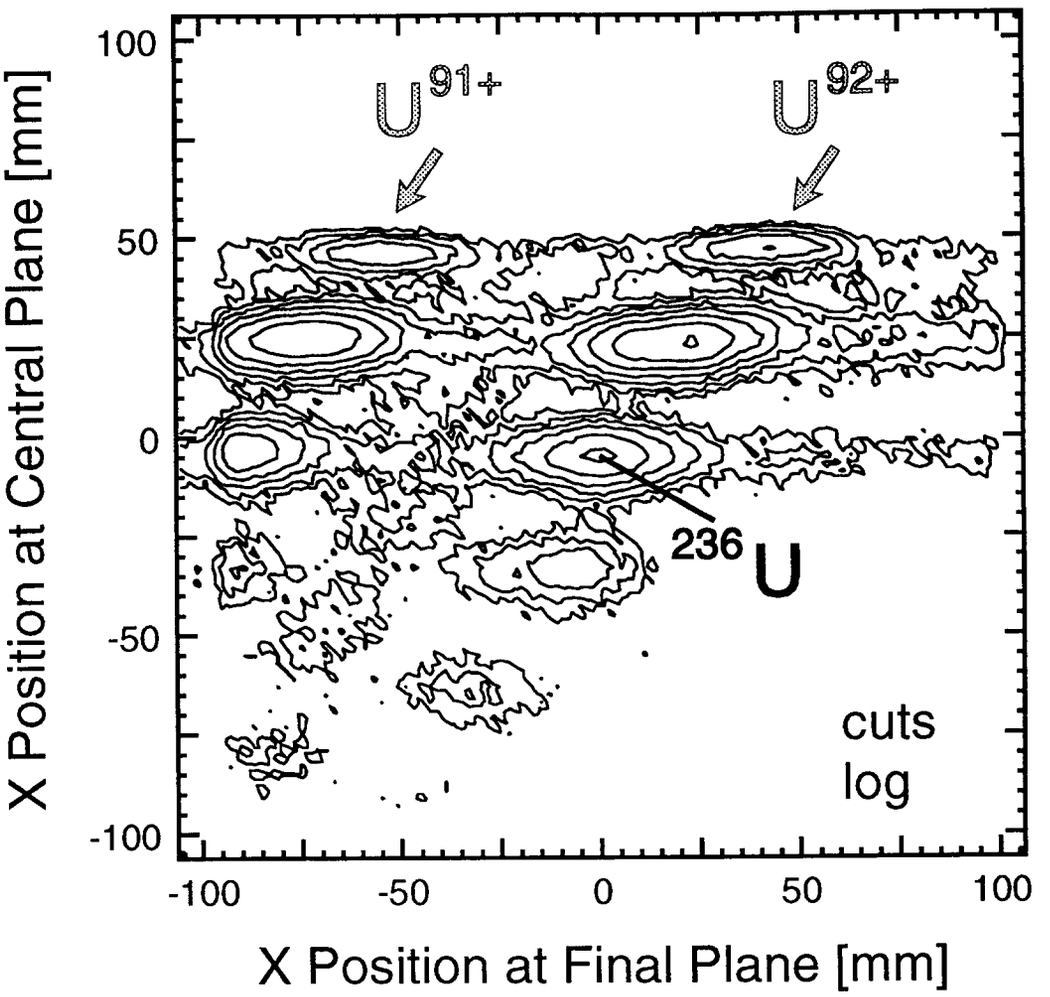

Fig. 5. Position distribution of the 950 A·MeV uranium fragments recorded at the central plane F_2 and at the final plane F_4 of the fragment separator.

calculated results from MOCADI are shown in fig. 6c. The overall agreement between calculation and experiment is quite good indicating that the atomic and nuclear kinematics are correctly implemented in the code.

For some experiments it is important to provide a beam of one single isotope at the exit of the FRS, e.g. for implantation and half-life determination. This can be done by removing all other fragments using the slit systems at F_2 and F_4. In figure 6b this is illustrated by selecting only those isotopes of figure 6a which are in between the two dashed horizontal lines indicating a possible setting of the slits at F_2. This figure shows the fragment distribution obtained at the final plane under that condition. The selected isotope ^{236}U is well separated from all the other isotopes. The result of the MOCADI calculation is shown on the right-hand side in figure 6d.

In figure 6 it is striking that the production cross sections for the one and two

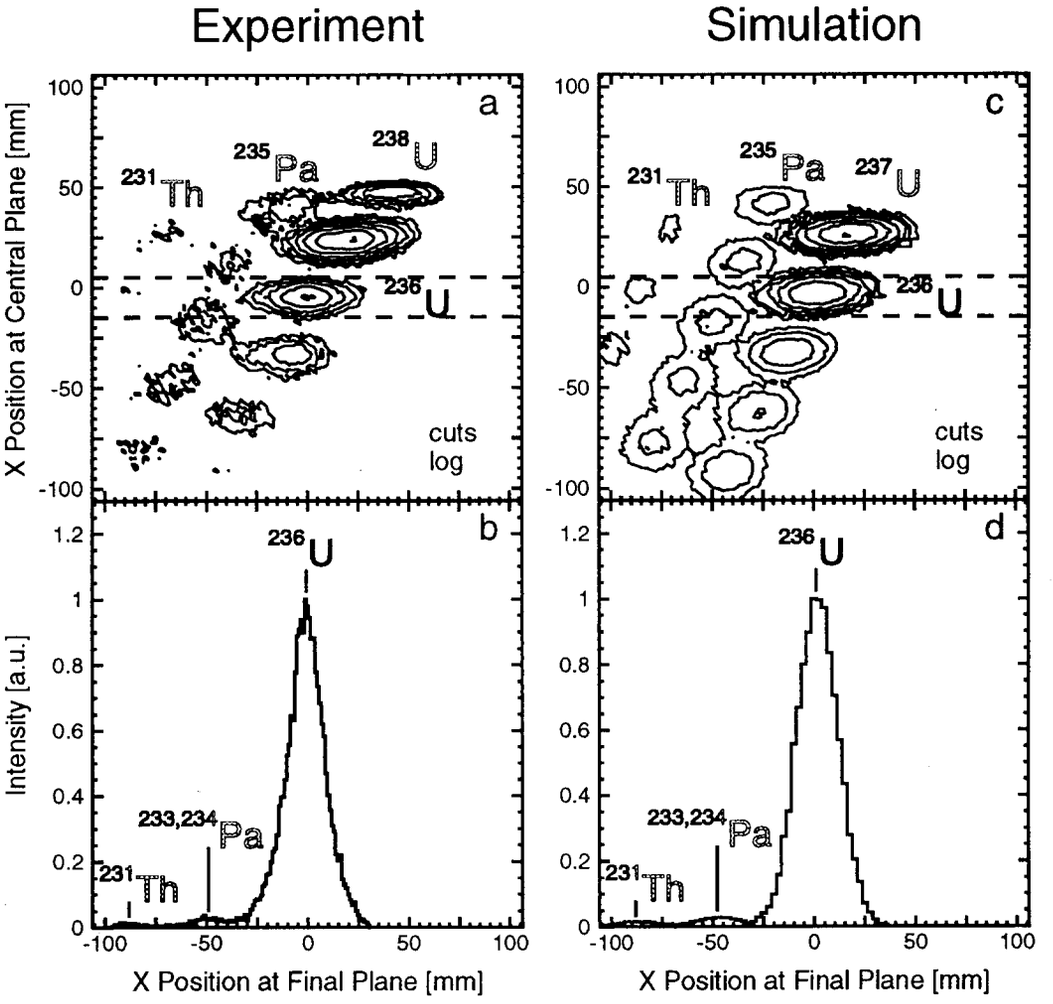

Fig. 6. (a) Position distribution of the uranium fragments after removing the contaminants due to hydrogen-like and helium-like ionic charge states. (b) Position distribution of the fragments at the final plane obtained with the horizontal slits at the central plane adjusted to the positions indicated by the dashed lines in the upper picture. A simulation of the experiment using the program MOCADI [16] is shown in part (c) and (d) of the picture.

neutron removal channels are enhanced compared to the production cross sections for the other fragments. The explanation is that these two nuclides are dominantly produced by electromagnetic dissociation after deexcitation of the giant dipole resonance and to a smaller contribution by the giant quadrupole resonance. The 3n fragmentation channel, however, cannot be explained by single-step electromagnetic excitations only. There is strong evidence that the double giant dipole resonance contributes to the 3n channel [30,31]. The momentum distributions are signatures of the different nuclear reaction mechanisms, this topic will be discussed in a forthcoming publication.

4 Summary and Outlook

With the spatial separation of relativistic uranium isotopes we have successfully verified a main design goal of the FRS. Isotopically pure secondary beams throughout the whole periodic table up to uranium can now be provided for the first time using the Bρ-ΔE-Bρ method. It should be mentioned that the same method has been applied to separate neutron-rich fragments created by projectile fission of relativistic uranium beams [32]. In a first pilot study we have proven that this reaction has produced about 40 new neutron-rich isotopes.

Decay studies with implanted nuclei have shown that due to the clean separation half-lives can be extracted already from the decays of few atoms [33].

Already the first experiments at the projectile fragment separator have shown new perspectives of secondary-beam physics at relativistic energies. The isotopically separated uranium projectile fragments produced in the recent experiment were used to study low-energy fission in a large range of nuclei from lead up to uranium which was not accessible before [34].

The storage ring ESR with its cooling facilities can be used to increase the phase-space density of the hot fragment beam by several orders of magnitude down to a transverse emittance below 0.05 π mm mrad and a relative momentum spread below 10^{-5} depending on the beam intensity [35]. High-resolution experiments can be performed by using either the internal gas-target in the ring or the extracted beam. The first injection of secondary beams from the FRS into the ESR has already shown the unique features of this combination [36].

The new exit of the FRS, presently under construction (see fig. 1), will provide secondary beams for exclusive experiments in the target hall using e.g. the large neutron detector LAND [37], the magnetic spectrometer ALADIN [38], or the spectrometer KAOS [39]. First experiments with the FRS in combination with the facilities LAND and ALADIN have also been successfully started to study the halo structure of very neutron-rich light nuclei [40].

The projectile fragment separator FRS is a central part of the new heavy-ion secondary-beam program at GSI. In its combination with the other high-energy facilities it allows new experimental techniques and provides access to information on nuclear structure and decay which was not accessible before.

Acknowledgement

We acknowledge the technical support of K.-H. Behr, A. Brünle, K.-H. Burkhard and the technical staff of GSI during the preparation of the experiment. Furthermore we would like to thank the GSI target laboratory for the preparation of the targets and the degrader layers with the necessary precision as well as the accelerator staff for fruitful collaboration during the experiment.

References

[1] D. E. Greiner, P. J. Lindstrom, H. H. Heckman, B. Cork, and F. S. Bieser, Phys. Rev. Lett. 35 (1975) 152.

[2] E. M. Friedlander and H. H. Heckman, Relativistic heavy-ion collisions: Experiment, in *Treatise on Heavy Ion Science*, edited by D. A. Bromley, vol. 4, Plenum Press, New York (1985) 403.

[3] J. P. Dufour, R. D. Moral, H. Emmermann, F. Hubert, D. Jean, C. Poinot, M. S. Pravikoff, A. Fleury, H. Delagrange, and K.-H. Schmidt, Nucl. Instr. Meth. A248 (1986) 267.

[4] H. Geissel et al., Nucl. Instr. Meth. B70 (1992) 286.

[5] K.-H. Schmidt et al., Nucl. Phys. A542 (1992) 699.

[6] F. Bosch, Nucl. Instr. Meth. A314 (1992) 269.

[7] K. Blasche and B. Franczak, in *Proc. of the third European Part. Acc. Conf., Berlin, 24-28 March, 1992*, edited by H. Henke, H. Homeyer, and C. Petit-Jean-Genaz, Editions Fronitière, Gif-Sur-Yvette (1992) 9.

[8] B. Franzke, Nucl. Instr. Meth. B24/25 (1987) 18.

[9] G. Münzenberg, Nucl. Instr. Meth. B70 (1992) 265.

[10] H. Wollnik, *Manual for GICO*, Univ. Gießen (1990), (unpublished).

[11] K.-H. Schmidt, E. Hanelt, H. Geissel, G. Münzenberg, and J. P. Dufour, Nucl. Instr. Meth. A260 (1987) 287.

[12] H. Geissel, T. Schwab, P. Armbruster, J. P. Dufour, E. Hanelt, K.-H. Schmidt, B. Sherrill, and G. Münzenberg, Nucl. Instr. Meth. A282 (1989) 247.

[13] W. Enghardt et al., Phys. Med. Biol. 37 (1992) 2127.

[14] C. Scheidenberger et al., accepted for publication in Phys. Ref. Lett. (1994).

[15] C. Scheidenberger et al., Nucl. Instr. Meth. B90 (1994) 36.

[16] T. Schwab, PhD thesis, Univ. Gießen (1990), GSI-Report GSI-91-10 (1991).

[17] S. Kox, A. Gamp, R. Cherkaoui, A. J. Cole, N. Longequeue, J. Menet, C. Perrin, and J. B. Viano, Nucl. Phys. A420 (1984) 162.

[18] K. Sümmerer, W. Brüchle, D. J. Morrissey, M. Schädel, B. Szweryn, and Y. Weifan, Phys. Rev. C42 (1990) 2546.

[19] C. A. Bertulani and G. Baur, Phys. Rep. 163 (1988) 299.

[20] D. Morrissey, Phys. Rev. C39 (1989) 460.

[21] H. Gould, D. Greiner, P. Lindstrom, T. J. M. Symons, and H. Crawford, Phys. Rev. Lett. 52 (1984) 180.

[22] T. Stöhlker et al., Nucl. Instr. Meth. B61 (1991) 408.

[23] R. Anhold, W. E. Meyerhof, H. Gould, C. Munger, J. Alonso, P. Thieberger, and H. E. Wegner, Phys. Rev. A32 (1985) 3302.

[24] C. Ziegler, T. Brohm, H.-G. Clerk, H. Geissel, K.-H. Schmidt, K. Sümmerer, D. J. Vieira, and B. Voss, GSI Scientific Report 1990, GSI-91-1 (1991) 291.

[25] A. Albert, K. Kroneberger, O. Heil, K. O. Groeneveld, and H. Geissel, Nucl. Instr. Meth. A317 (1992) 397.

[26] H. Folger, H. Geissel, W. Hartmann, J. Klemm, G. Münzenberg, D. Schardt, K.-H. Schmidt, and W. Thalheimer, Nucl. Instr. Meth. A303 (1991) 24.

[27] B. Voss et al., GSI Scientific Report 1988, GSI-89-1 (1989) 283.

[28] H. Stelzer, Nucl. Instr. Meth. A310 (1991) 103.

[29] M. Pfützner, H. Geissel, G. Münzenberg, F. Nickel, C. Scheidenberger, K.-H. Schmidt, K. Sümmerer, T. Brohm, B. Voss, and H. Bichsel, Nucl. Instr. Meth. B86 (1994) 213.

[30] T. Aumann et al., GSI Scientific Report 1993, GSI-94-1 (1994) 69.

[31] T. Aumann, J. V. Kratz, E. Stiel, K. Sümmerer, W. Brüchle, M. Schädel, G. Wirth, M. Fauerbach, and J. C. Hill, Phys. Rev. C47 (1993) 1728.

[32] M. Bernas et al., accepted for publication in Phys. Lett. B (1994).

[33] S. Czajkowski et al., Z. Phys. A348 (1994) 267.

[34] K.-H. Schmidt et al., Phys. Lett. B325 (1994) 313.

[35] M. Steck et al., in *Proc. of the third European Part. Acc. Conf., Berlin, 24-28 March, 1992*, edited by H. Henke, H. Homeyer, and C. Petit-Jean-Genaz, Editions Fronitière, Gif-Sur-Yvette (1992) 827.

[36] H. Geissel et al., Phys. Rev. Lett. 68 (1992) 3412.

[37] T. Blaich et al., Nucl. Instr. Meth. A314 (1992) 136.

[38] J. Hubele et al., Z. Phys. A340 (1991) 263.

[39] P. Senger et al., Nucl. Instr. Meth. A327 (1993) 393.

[40] F. Humbert et al., GSI Scientific Report 1993, GSI-94-1 (1994) 14.